PLASMA DYNAMICS

# VII. PLASMA PHYSICS*


Prof. S. C. Brown
Prof. G. Bekefi
Prof. K. U. Ingard
Prof. D. R. Whitehouse
Dr. J. C. Ingraham
M. L. Andrews
F. X. Crist
J. K. Domen
E. W. Fitzgerald, Jr.
G. A. Garosi
W. H. Glenn, Jr.
E. B. Hooper, Jr.
P. W. Jameson
J. J. Linehan
D. T. Llewellyn-Jones
E. M. Mattison
J. J. McCarthy
W. J. Mulligan
J. J. Nolan, Jr.
G. L. Rogoff
D. W. Swain
F. Y-F. Tse
B. L. Wright


## A. IMPURITY PHOTOCONDUCTION OF InSb IN MAGNETIC FIELDS

As a semiconductor with detector applications in the infrared, InSb has attracted attention not only at wavelengths of 8 μ and less, where intrinsic photoconductivity occurs, but also from 60 μ to 8 mm. At pumped liquid-helium temperatures below 1.9°K and in magnetic fields above 5 kG the resistance of a low-impurity concentration n-type InSb crystal is decreased when far infrared radiation is incident on it and the response time is less than 1 μsec. We have investigated the impurity photoconductivity of n-type InSb in a magnetic field which we find accounts for the change in conduction of the InSb irradiated by infrared from 60 μ to 230 μ. The two fortunate properties of InSb which make it responsive at these wavelengths are its high dielectric constant and its low effective mass. A good measurement of the latter can be derived from the dependence of this impurity photoconductivity on magnetic field.

In the course of using an InSb detector for the far infrared, 60-230 μ, it was noted that the response of the detector has a definite peak in the frequency spectrum and that the frequency at which the response peaks is a function of magnetic field. The detector consists of an n-type InSb crystal[1] with impurity concentrations of $3 \times 10^{13}$ cm$^{-3}$ and a free carrier mobility greater than $5 \times 10^{5}$ cm$^{2}$ V$^{-1}$ sec$^{-1}$ at 77°K. This 5 × 5 × 2 mm crystal is polished on one 5 × 5 mm side that is placed perpendicular to a noncondensing light pipe, thereby introducing the far infrared radiation within a cone whose angular spread is less than 9° from the normal. Surrounding the crystal is a superconducting solenoid magnet that can produce a field perpendicular to the crystal surface of 0-20 kG. The detector is immersed in a liquid-helium dewar and operated at pumped helium temperature of 1.78 ± .03°K. Two leads on opposite 5 × 2 mm sides of the crystal allow measurement of the conductivity by chopping the imput infrared at 1.8 kc and synchronously detecting crystal resistance, thereby eliminating zero shifts from thermal effects.

A high-pressure mercury arc served as the far infrared source, and this radiation passed through a Perkin-Elmer grating monochrometer that gave a slit limited resolution $d\lambda/\lambda$ of 6 per cent from 60-230 μ, with two gratings of 6.4 and 3.2 lines per mm used. Any radiation below 8 μ which produces intrinsic photoconductivity for InSb was


*This work was supported in part by the U.S. Atomic Energy Commission (Contract AT(30-1)-1842).

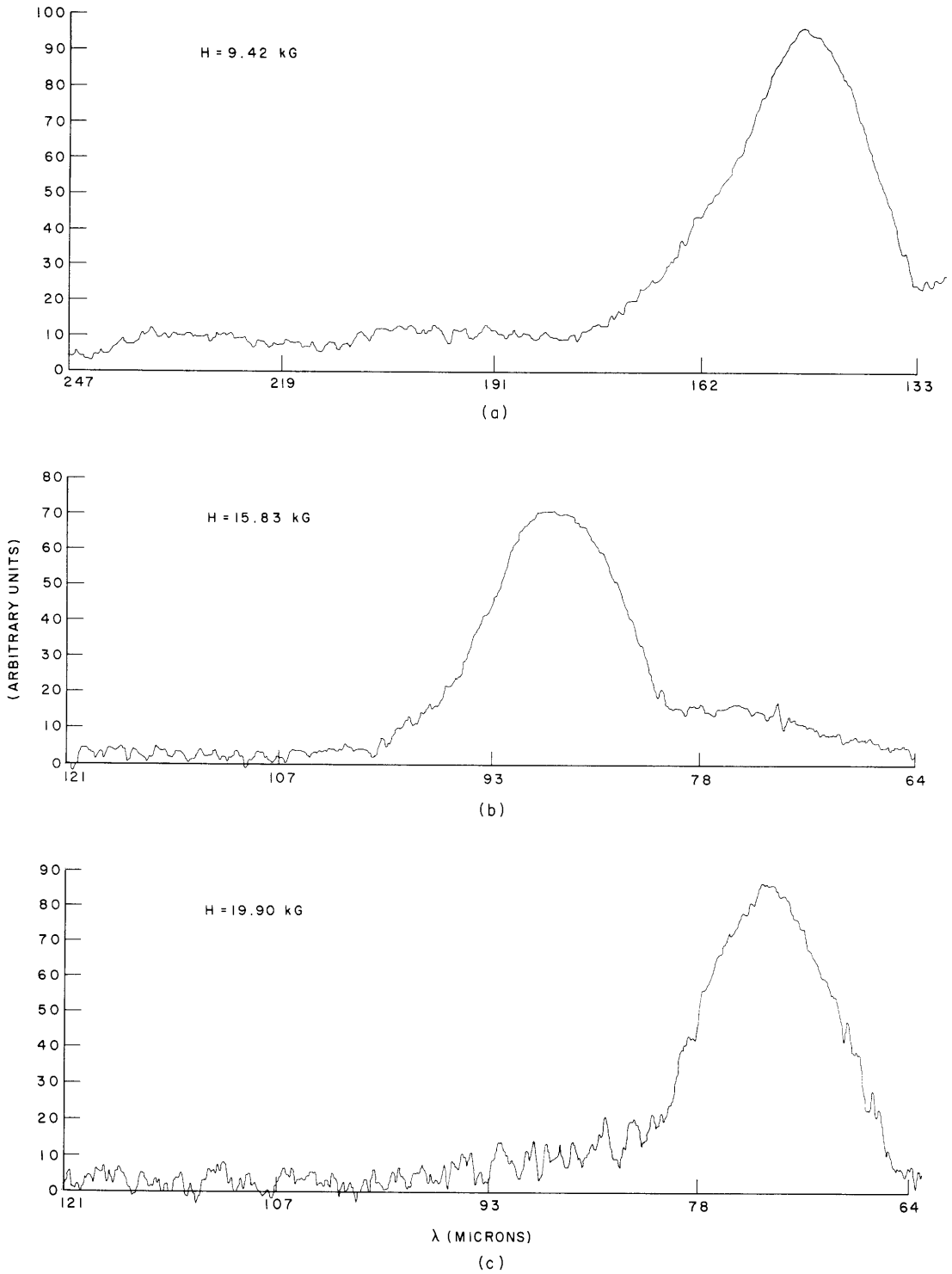


Fig. VII-1. Detector output as a function of frequency of the incident infrared for three magnetic fields.

eliminated by a 12-mil thick filter of black polyethylene, and the detector was insensitive from 8 μ to 60 μ, so there was no problem of higher diffraction orders of shorter wavelengths overlapping the spectra.

In Fig. VII-1 samples of spectra for three magnetic fields show this insensitivity peak and indicate at what frequency the impurity photoconductivity is maximum for the given magnetic fields. This frequency plotted as a function of magnetic field is shown in Fig. VII-2 for all of the experimental data. Further investigation was made to determine whether or not the polarization of the incident radiation had any effect. Inside the

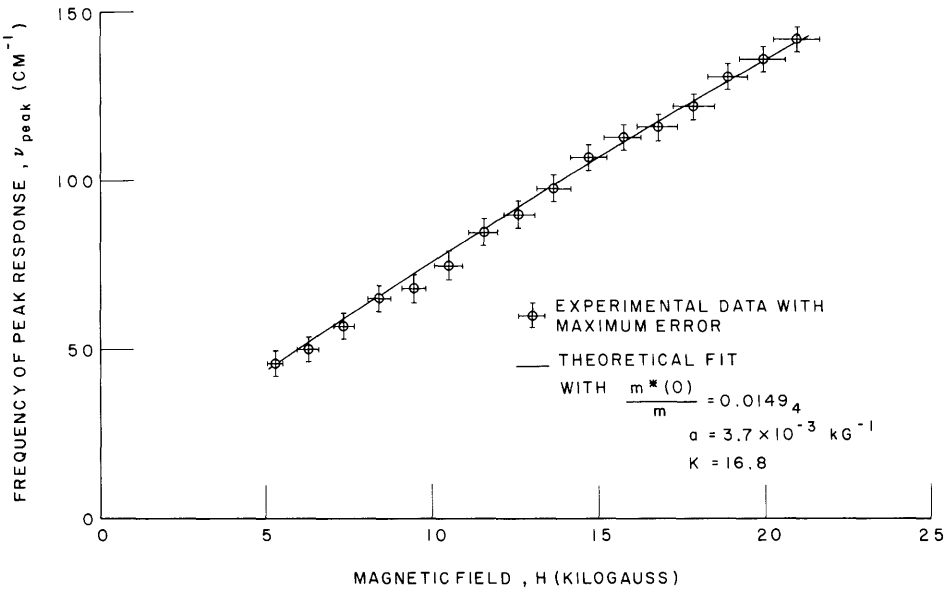


Fig. VII-2. The frequency of the peak in detector output as a function of magnetic field compared with theory.

magnet immediately before the crystal a crude polarizer, consisting of one layer of clear polyethelene, 32 μ thick, held at the Brewster angle followed by a 2.47-mm thick plate of crystal quartz serving as a quarter-wave plate for 138 μ, was placed. The polyethylene gave a small percentage linear polarization superimposed on the random polarization so that this same percentage — more right-handed circular polarization than left-handed — was incident on the crystal. Experimentally, the response of the detector to 138 μ was approximately 10 per cent more when the magnetic field was antiparallel to the direction of incidence of the infrared than when it was parallel. This indicates that the impurity photoconductivity occurs when the electric vector of the incident radiation rotates about the magnetic field in a right-handed sense.

From Fig. VII-2 it becomes obvious that this increased sensitivity cannot be due to enhanced absorption from cyclotron resonance because there is a positive intercept at

zero magnetic field. Neither can this be attributed to the plasma frequency, for there is no plasma frequency shift of the cyclotron frequency because the incident radiation is along the magnetic field and the sample is large compared with a wavelength. That simple cyclotron resonance cannot be the cause is reasonable, since at 1.78°K the number of electrons in the conduction band is much less than the number captured by donor atoms. The increased conduction caused by the infrared radiation may be caused by photoionization of electrons from donor atoms into the conduction band. The binding energy of the electron in the ground state of the donor atom has been worked out by Y. Yafet, R. W. Keyes, and E. N. Adams,[2] using the approximation of a hydrogen atom in a high magnetic field, the electron having the effective mass of InSb and the system being immersed in a dielectric whose constant is that of InSb. Further work on the other states of the electron and the selection rules for transitions have been worked out by R. F. Wallis and H. J. Bowlden.[3] The two possible transitions are from the ground state of the donor atom and from the first excited state of the donor atom of the second Landau-level conduction band. Both of these transitions occur when the electric vector of the incident radiation rotates about the magnetic field in a right-handed sense. Under the assumption that there are enough impurity acceptor atoms present to hold the Fermi level as low as the ground state of the donors, the Fermi distribution is well approximated by the Boltzmann distribution which determines from the energy difference between the ground and first excited state of the donor atom that the population of the ground state is more than one hundred times that of the next higher state for the magnetic fields employed. The calculations of Yafet, Keyes, and Adams[2] for the binding energy of the ground state, which are good to 15 per cent even at zero magnetic field (and improve as magnetic field increases), can be fitted by a parabolic energy dependence that is good within 2 per cent of the calculations for magnetic fields used.

$$E_B = 0.777\left[\mu_B H \frac{R_y}{K^2}\right]^{1/2} + 1.00 \frac{R_y}{K^2}\frac{m^*}{m},$$

where $E_B$ is the binding energy of the ground state of the donor atom relative to the conduction band of the first Landau level, H is the magnetic field, $\mu_B$ is the Bohr magneton, $R_y$ is the Rydberg constant, K is the dielectric constant of InSb for frequencies $E_B/h$, and $m^*/m$ is the ratio of effective electron mass in isotropic InSb to the free electron mass. If the nonparabolic nature of the energy bands is taken into account, the energy of the Landau-level conduction bands from the bottom of the conduction band is that given by Lax, Mavroides, Zeiger, and Keyes.[4]

This has the form

$$E_{n\,\updownarrow} = \mu_B H\left[(2n+1)\frac{m}{m^*} \pm g^*\right],$$

where $g^*$ is the effective spectroscopic splitting factor, and, for our magnetic fields,

$$\frac{m}{m^*}=\frac{m}{m^*_{(o)}}\left[1-0.92\frac{E_{n\updownarrow}}{E_g}\right]$$

and

$$g^* = g^*_{(o)}\left[1-1.20\frac{E_{n\updownarrow}}{E_g}\right].$$

Here, the subscript (o) refers to the bottom of the conduction band and we have taken the values of the energy gap, $E_g = 0.24$ ev, and the spin-orbit splitting, $\lambda = 0.9$ ev. Defining $\alpha$ and $\gamma$ by

$$\frac{m}{m^*} = \frac{m}{m^*_{(o)}}[1-\alpha E_{n\updownarrow}]$$

and

$$g^* = g^*_{(o)}[1-\gamma E_{n\updownarrow}],$$

we obtain

$$E_{n\updownarrow} = \frac{\mu_B H\left[(2n+1)\frac{m}{m^*_{(o)}} \pm g^*_{(o)}\right]}{1+\mu_B H\left[(2n+1)\,\alpha\frac{m}{m^*_{(o)}} \pm \gamma g^*_{(o)}\right]}$$

and

$$(E_{1\uparrow}-E_{o\uparrow}) = 2\mu_B H\frac{m}{m^*_{(o)}}\left\{1-\mu_B H\left[4\alpha\frac{m}{m^*_{(o)}}+(\alpha+\gamma)g^*_{(o)}\right]\right\}$$

with an error from approximations of less than 1.2 per cent even at our highest field of 21 kG. The ground state of the donor atom is so close to the bottom of the conduction band that the variation of effective mass for it is negligible, so that the complete transition is expressed as

$$(E_{1\downarrow}-E_{o\downarrow}+E_B) = 2\mu_B H\frac{m}{m^*_{(o)}}\left\{1-\mu_B H\left[4\alpha\frac{m}{m^*_{(o)}}+(\alpha+\gamma)g^*_{(o)}\right]\right\}+0.777\left[\mu_B H\frac{R_y}{K^2}\right]^{1/2}$$
$$+1.00\frac{R_y}{K^2}\frac{m^*_{(o)}}{m}.$$

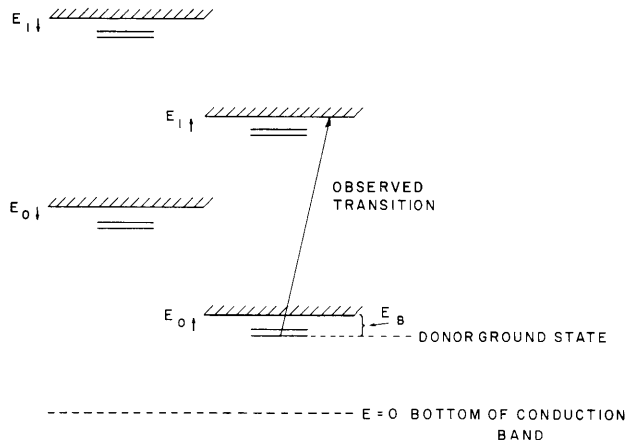


Fig. VII-3.
Schematic representation of the energy levels of InSb in a magnetic field.

This transition is shown schematically in Fig. VII-3 by an energy-level diagram giving the relative position of neighboring levels. To fit this dependence as

$$\nu_{peak} = 2\mu_B H \frac{m}{m^*_{(o)}}[1-aH] + 0.777\left[\mu_B H \frac{R_y}{K^2}\right]^{1/2} + 1.00 \frac{R_y}{K^2}\frac{m^*_{(o)}}{m} \qquad (1)$$

to the experimental data, the dielectric constant, K, and the variation of effective mass with energy, a, are needed. Since the fundamental lattice vibration occurs at ~189 $cm^{-1}$, $K(E_B/h) = K(o)$. Optical measurements of $K(\infty)$ give ~15.2 at room temperature, while Fray, Johnson, and Jones[5] obtain a maximum $(K(o)-K(\infty))$ of 1.3, and Spitzer and Fan[6] a maximum of 1.5. Therefore a K(o) of 16.8 seems reasonable, although there are some widely different published values. For a value of a, extrapolating the data of Lax et al.[4] at room temperature to our magnetic fields, we find $7.4 \times 10^{-3}$ $kG^{-1}$ while, from their theory as given here with $E_g = 0.24$ ev and $\lambda = 0.9$ ev at helium temperatures, $a = 3.7 \times 10^{-3}$ $kG^{-1}$. Also, Palik, Picus, Teitler, and Wallis,[7] at magnetic fields in our range and liquid-nitrogen temperatures, obtain $a = 4.8 \times 10^{-3}$ $kG^{-1}$. In Table VII-1, values of $m^*_{(o)}/m$ are given from the best fit of Eq. 1 to the experimental data, with the indicated values of K and a assumed.

Table VII-1. Values of $m^*_{(o)}/m$.

| | | K | | |
|---|---|---|---|---|
| | | 16.0 | 16.8 | 17.6 |
| a | $3.0 \times 10^{-3}$ $kG^{-1}$ | $0.0153_6$ | $0.0151_8$ | $0.0150_0$ |
| | $3.7 \times 10^{-3}$ $kG^{-1}$ | $0.0151_3$ | $0.0149_4$ | $0.0148_2$ |
| | $4.4 \times 10^{-3}$ $kG^{-1}$ | $0.0148_8$ | $0.0147_3$ | $0.0145_9$ |

Lax et al.[4] extrapolating to T = 4.0°K with $E_g$ = 0.24 and $\lambda$ = 0.9 find $m^*_{(o)}/m$ = 0.0155, and that Palik et al.[7] at T = 80°K obtain $m^*_{(o)}/m$ = 0.0145, pointing out that if only the dilational part of $E_g$ is used, the theoretical extrapolation gives $m^*_{(o)}/m$ = 0.0145, Therefore our value of $m^*_{(o)}/m$ = 0.0150 ± .0008 seems reasonable, and from the theoretical fit shown in Fig. VII-2 the mechanism of impurity photoconductivity from the ground state of the donor atom to the second Landau-level conduction band accounts very well for the conductivity dependence of infrared irradiated InSb in a magnetic field. The frequency selectivity of this mechanism holds promise for a tunable detector in the far infrared.

M. L. Andrews

## References

1. This crystal with measurements of its impurity concentration and free carrier mobility were kindly given to us by the Mullard Laboratories of England.

2. Y. Yafet, R. W. Keyes, and E. N. Adams, J. Phys. Chem. Solids 1, 137 (1956).

3. R. F. Wallis and H. J. Bowlden, J. Phys. Chem. Solids 7, 78 (1958).

4. B. Lax, J. G. Mavroides, H. J. Zeiger, and R. J. Keyes, Phys. Rev. 122, 31 (1961).

5. S. J. Fray, F. A. Johnson, and R. H. Jones, Proc. Phys. Soc. (London) 76, 939 (1960).

6. W. G. Spitzer and H. Y. Fan, Phys. Rev. 99, 1893 (1955).

7. E. D. Palik, G. S. Picus, S. Teitler, and R. F. Wallis, Phys. Rev. 122, 475 (1961).

## B. STEADY-STATE BEAM PLASMA DISCHARGE

Preliminary observations have been made of steady-state characteristics of the discharge and of possible loss mechanisms. The system employs a stainless-steel chamber, 5 inches in diameter, a solenoid that permits radial access through 5 ports, a vacuum system with a base pressure of $2 \times 10^{-6}$ mm, and symmetrical Armco-iron pole pieces, one of which shields a Pierce electron gun that can be operated with pulse lengths from a few microseconds to four milliseconds or can run at DC gun voltages up to 1600 volts. The gun was usually operated at 800 volts with a total current of 25 ma because higher voltages usually only increased the intensity of the observed phenomena. The anode, the collector at the other pole piece, and the wall chamber are grounded through resistors.

The pressure range used is from 1 to $6 \times 10^{-4}$ mm in a vacuum system of continuously pumped argon. The distance between pole pieces is 20 inches, and a mirror is formed by two end magnets over the pole pieces.

The operating region has the following initial characteristics: Approximately 2 μsec

after the beam is turned on, a uniform oscillation of several megacycles occurs in the collector and wall circuits and lasts for several microseconds. Thereupon there is a violent disruption of both currents and the trace continues to be erratic for approximately 40 μsec. Thereafter the light intensity rises very rapidly, the collector current becomes more negative, and the wall current becomes positive. A steady state is soon reached. The beam plasma, purple in color, varies in diameter with the applied axial magnetic field.

When the central field exceeds ~60 gauss, the plasma in the steady state is characterized by an m = 2 mode right-handed rotation that is reversible when the applied magnetic field is reversed and has a 1-2 kc/sec frequency. No axial variation in rotation is observed. The frequency of rotation is found to be inversely proportional to magnetic field and pressure, and directly proportional to the applied gun voltage. If this is due to an E × B drift, an inward radial E field is required. Plasma potential differences are being determined. The plasma potential in the region outside the luminous core of the discharge is ~+24 volts. The floating potential is positive, decreasing with decreasing radius and becoming negative only near the axis. The rotation becomes very clear when the floating potential remains rather constant through most of the radial distance. Investigation by a probe shows that this two-spoke rotation, which is predominant in the system, extends to the core of the discharge.

1. Oscillograms and Preliminary Experimental Results

All the oscillograms have a 0.5 msec/cm time scale, except the third which has 0.2 msec/cm. Positive current is always read upward. The applied gun voltage is 800 volts. The photomultiplier looks though a slit parallel to the axis near the center of the discharge. Current to the cylindrical wall is sampled by copper plates, 3/4 inch square, tangent to the chamber wall, and grounded through resistors. The plate positions are indicated in the diagrams and the numbers refer to the corresponding traces. (Upper trace is number 1.)

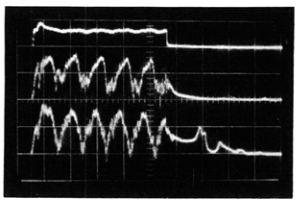

Fig. VII-4. Photomultiplier response and the large-scale rotation in the discharge (140 gauss). Mirror ratio = 2.4. Upper trace: photomultiplier output. Middle and lower traces: currents to wall plates.

The pulse length in Fig. VII-4 is 2.5 msec. Though the gain for the photomultiplier trace has been kept low to keep the trace on the screen, the usual general pattern can be seen. The light intensity drops slightly after initiation of the large-scale rotation a few microseconds after the start of the beam pulse. The mechanism that expands the plasma into radial arms may account for the decrease.

The two lower traces show the pulses of positive current to two of the copper plates. The peak current is +0.3 ma. Note the flow of current to the wall after the end of the pulse (abrupt photomultiplier trace ending) and the semblance of persisting rotation.

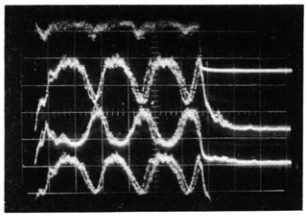

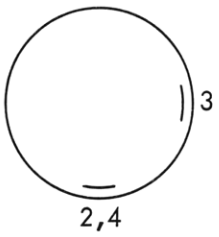


Fig. VII-5. Modulated photomultiplier response and phase relations of wall currents (218 gauss). Mirror ratio = 1.6. First trace: photomultiplier output showing light intensity modulated at the same frequency as the rotation. Second and fourth traces: currents to two plates along the same axial position. Third trace: current to plate located geometrically 90° away.

A four-trace preamplifier unit is used here, with the chopped mode to observe the phase relations of the positive currents to the plates. The second and fourth traces show no phase change of rotation in the axial direction. (Nor was any change observed when a series of closely separated plates was placed along a 12-inch distance down the chamber wall.) The m = 2 mode is indicated by the third trace, as the current is 180° out of phase with the other two, though the plate is only at a right angle to the other two axially positioned plates.

Optical evidence for the rotation is seen in the upper trace; thus it might be assumed that the two spokes alternately move into the field of view and cause an intensity modulation. With different operating conditions (pressure, magnetic field, and voltage) and photomultiplier position, a much stronger modulation, which still has the frequency of the positive-plate currents, can be observed.

In Fig. VII-6 the first and fourth traces are from opposite plates, though the phase factor is not quite clear in this particular oscillogram. A plate at 45° (third trace) was used to determine the rotation direction. Under all operating conditions investigated, an inward radial E field is needed if we assume an E × B drift.

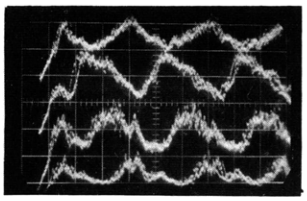

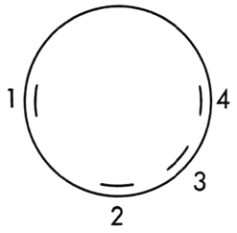


Fig. VII-6.

Current-phase relations for determining rotation direction (197 gauss). Mirror ratio = 1.8. Currents to wall plates as indicated. Currents to plates on opposite sides of the chamber are in phase.

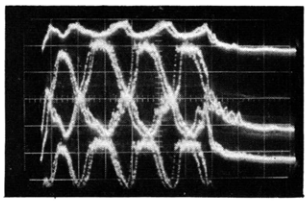

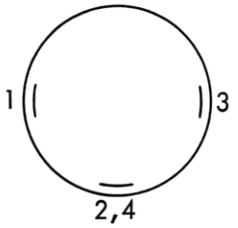


Fig. VII-7.

Current-phase relations for the m = 2 mode (215 gauss). Mirror ratio = 2.5. Currents to wall plates as indicated.

The phase relations of the currents in Fig. VII-7 again illustrate the m = 2 mode. Currents to opposite sides of the chamber (first and third traces) are in phase. Currents to plates at right angles (first or third, with second or fourth) are 180° out of phase. Currents in the axial direction (second and fourth traces) are in phase. The double image is due to a double exposure.

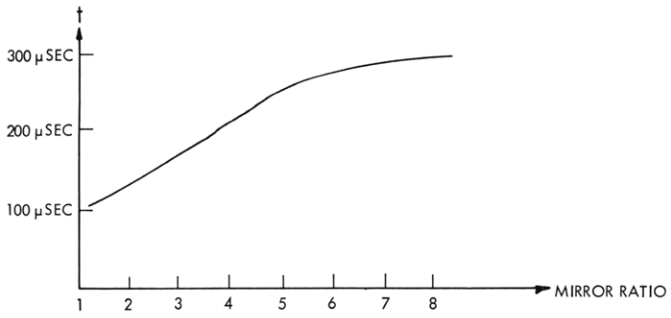


Fig. VII-8.

Containment effect of the mirror after end of pulse. (Pressure, $2 \times 10^{-4}$ mm; t is time for current to fall to 1/e.)

Positive current flow to the cylindrical wall persists after the end of the pulse. The effect of the mirror for one operating region is plotted in Fig. VII-8 for a constant central field of 130 gauss.

J. K. Domen

## C. LASER INTERFEROMETER

### 1. Introduction

An interferometer to measure dielectric constants in the visible and near infrared has been constructed. It is intended for use in the study of high-density plasmas. The present report, however, discusses only the interferometer.

The interferometer is a modification of one first developed by Ashby and Jephcott.[1] They found that if the light emitted by a laser is reflected back into the laser, the amplitude of the laser is changed by an amount that depends on the phase of the returning light. Thus, if a time-variant dielectric is placed between the external reflector and the laser, the light output will vary in time with the dielectric. Ashby and Jephcott used this technique to measure changes of several fringe shifts, that is, phase changes larger than $2\pi$. Gerardo and Verdeyen[2] made the technique more sensitive by a technique which essentially amounts to passing the light through the medium several times, yielding an increase in sensitivity approaching two orders of magnitude.

The present interferometer is capable of measuring dielectric constants that are repetitive in time. Both a plasma and a calibrated compensator dielectric are placed between the laser and the external mirror. In the absence of the compensator, the laser beam is modulated at the same frequency as the plasma. The dielectric constant of the compensator is varied at the same rate as the plasma, and adjusted so that the laser output contains no component at the modulation frequency. The dielectric constant is then equal to the negative of that of the compensator. On the basis of the experimental work up to this time, the device appears to be capable of measuring phase changes considerably smaller than $2\pi \times 10^{-2}$.

### 2. Theory of the Interferometer

The characteristic modes of laser cavities have been determined.[3,4] The three-cavity system can be analyzed in terms of these modes. Describe the electric field amplitude on mirror j that is due to the field on mirror i by an operator $O_{ij}$, which can be derived by simple diffraction theory. Then

$$u_j(\vec{r}_j) = O_{ji} u_i(\vec{r}_i), \tag{1a}$$

where r is a vector on the surface of the mirror. In the simple case of a plane wave propagating between the two mirrors, $O_{ji}$ is just the phase factor and

$$u_j(\vec{r}_j) = e^{-ikd_{ij}} u_i(\vec{r}_i), \tag{1b}$$

where k is the wave number, $2\pi/\lambda$, and $d_{ij}$ is the distance between the two mirrors.

In the more general case, Boyd, Gordon, and Kogelnik[3, 4] found that the field induced on i after reflection from j can be written

$$O_{ij}O_{ji}u_i = D_{ij} \exp\left\{-i\left[2kd_{ij} - 2(1+m+n)\cos^{-1}\sqrt{\left(1-\frac{d_{ij}}{b_i}\right)\left(1-\frac{d_{ij}}{b_j}\right)}\right]\right\} u_i, \qquad (2)$$

where $b_i$ and $b_j$ are the radii of curvature of the two mirrors (see Fig. VII-9a). The $D_{ij}$ is a real number $\lesssim 1$, and contains the diffraction losses of the system. The

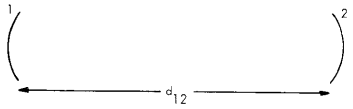


(a)

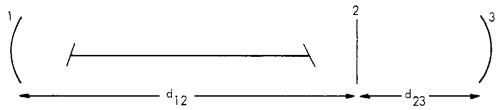


(b)

Fig. VII-9. (a) Two-mirror system. Mirror 1 has radius $b_1$, mirror 2 radius $b_2$. (b) Three-mirror system. The radii of curvature of the mirrors are $b_1$, $b_2 = \infty$, and $b_3$. Note the laser between 1 and 2.

characteristic modes of the system are found by setting Eq. 2 equal to $u_i$. Hence the phase factor in (2) is equal to $2\pi q$, so that

$$\frac{2\pi d_{ij}}{\lambda} = \pi q + (1+m+n)\cos^{-1}\sqrt{\left(1-\frac{d_{ij}}{b_i}\right)\left(1-\frac{d_{ij}}{b_i}\right)}. \qquad (3a)$$

Consider now the three-mirror system of Fig. VII-9b. The laser has a nonlinear gain, which can be represented by $\alpha - \beta|u|^2$. Experimentally, it is observed that the eigenmodes of the active laser are approximately those of the passive optical cavity, so that it is permissible to neglect the effect of the operator $O_{ij}$ on the nonlinear part of this gain. This is equivalent to neglecting mode pulling with the laser.

Let each mirror have a reflectance $r \lesssim 1$, and a transmittance $t = 1 - r$. Mirror 2

has light projected on it by both mirror 1 and mirror 3. For convenience, call the amplitude on the mirror 1 side of mirror 2 $u_2'$, and that on the mirror 3 side $u_2''$. Then the various amplitudes can be related as follows:

$$u_1 = r_1(a-\beta|u|^2)\, u_2' \tag{4a}$$

$$u_2' = r_2(a-\beta|u|^2)\, u_1 + t_2 u_2'' \tag{4b}$$

$$u_2'' = +r_2 O_{23} u_3 \tag{4c}$$

$$u_3 = r_3 O_{32} u_2'' + t_2 r_3 O_{32} u_2'. \tag{4d}$$

Solving for $u_2'$ and using Eq. 2, one obtains

$$\left\{1 - (a-\beta|u|^2)D_{12}r_1r_2\, e^{-i\phi_{12}} + \frac{t_2^2 r_2 r_3 D_{23}\, e^{-i\phi_{23}}}{1 - D_{23}r_2r_3\, e^{-i\phi_{23}}}\right\} u_2' = 0 \tag{5a}$$

with

$$\phi_{ij} = 2kd_{ij} - (1+m+n)\cos^{-1}\sqrt{\left(1 - \frac{d_{ij}}{b_i}\right)\left(1 - \frac{d_{ij}}{b_j}\right)}.$$

For the case in which the gain of the laser is zero, and the light is a plane wave, this becomes

$$\left\{1 - r_1r_2\, e^{-2ikd_{12}} + \frac{t_2^2\, e^{-2ikd_{23}}}{1 - e^{-2ikd_{23}}}\right\} u_2' = 0. \tag{5b}$$

Since the dielectric to be measured is inserted between mirrors 2 and 3, its effect can be represented as a change of $d_{23}$. Equation 5a yields

$$D_{12}r_1r_2(a-\beta|u|^2)^2 = \left(1 + \frac{t_2^2 r_2 r_3 D_{23}\, e^{-i\phi_{23}}}{1 - D_{23}r_2r_3\, e^{-i\phi_{23}}}\right) e^{i\phi_{12}}. \tag{6}$$

Taking the real and imaginary parts, one obtains

$$D_{12}r_1r_2(a-\beta|u^2)^2 = \cos\phi_{12} + t_2^2\, \mathrm{Re}\left[\frac{e^{i\phi_{12}}\, D_{23}r_2r_3\, e^{-i\phi_{23}}}{1 - D_{23}r_2r_3\, e^{-i\phi_{23}}}\right] \tag{7a}$$

$$0 = \sin \phi_{12} + t_2^2 \, \mathrm{Im}\left[\frac{e^{i\phi_{12}} D_{23} r_2 r_3 \, e^{-i\phi_{23}}}{1 - D_{23} r_2 r_3 \, e^{-i\phi_{23}}}\right]. \tag{7b}$$

Since $t^2$ is very small ($\sim 10^{-4}$), Eq. 7b shows that, except near the resonance of the second term, the characteristic modes of the three-mirror system occur at the same frequency as those of the laser itself (Eq. 3a). This is to be expected as this resonance occurs only when the characteristic modes of the mirror system 2-3 are excited, and only at this point can energy be strongly coupled into the optical cavity.

Even near the resonance of the 2-3 mirror system the frequency pulling of the laser is small, since the frequency of the laser is already close to the resonant frequency. Mathematically, this occurs because near this resonance $e^{-i\phi_{23}} \Big/ \left(1 - D_{23} r_2 r_3 \, e^{-i\phi_{23}}\right)$ has only a small imaginary part, so that Eq. 7b is approximately

$$0 = \left[1 + t_2^2 \, \mathrm{Re}\left(\frac{D_{23} r_2 r_3 \, e^{-i\phi_{23}}}{1 - D_{23} r_2 r_3 \, e^{-i\phi_{23}}}\right)\right] \sin \phi_{12}. \tag{7c}$$

One thus concludes that the characteristic frequencies of the three-mirror system are approximately those of the two-mirror system.

The laser intensity follows from (7a) and is

$$|u|^2 = |u_o|^2 + \frac{1}{\beta\sqrt{D_{12} r_1 r_2}}\left\{1 - \sqrt{1 + t_2^2 \, \mathrm{Re}\left[\frac{D_{23} r_2 r_3 \, e^{-i\phi_{23}}}{1 - D_{23} r_2 r_3 \, e^{-i\phi_{23}}}\right]}\right\} \tag{8}$$

where $|u_o|^2 = \frac{1}{\beta}\left(\alpha - \frac{1}{\sqrt{D_{12} r_1 r_2}}\right)$ is the laser intensity in the absence of the third mirror.

If we give $\phi_{23}$ a small time-dependent part, $\phi_{23} = \phi_{23}^o + \phi_{23}' s(t)$, the laser output will have a time dependence given by

$$\Delta|u_o|^2 = I\left(\phi_{23}^o\right) \phi_{23}' s(t) \tag{9a}$$

with $I\left(\phi_{23}^o\right)$ derived from Eq. 8

$$I\left(\phi_{23}^o\right) = \frac{1}{2}\frac{D_{23} r_3}{D_{12} r_1} \frac{t_2^2}{\beta^2\left(|u|^2 - \frac{\alpha}{\beta}\right)} \mathrm{Im}\left[\frac{-e^{-i\phi_{23}}}{\left(1 - D_{23} r_2 r_3 \, e^{-i\phi_{23}^o}\right)^2}\right]. \tag{9b}$$

In Eq. 9b, $|u|^2$ is evaluated at $\phi_{23} = \phi_{23}^o$. Near the resonance of the cavity 2-3, $e^{i\phi_{23}^o}$ is approximately real, so that I is small. The maximum signal will occur at $\phi_{23}^o = n\pi$ with n odd, that is, between the resonances of the cavity 2-3. Hereafter, it will be convenient to make the approximation

$$I\left(\phi_{23}^o\right) = I_o \sin \phi_{23}^o, \tag{9c}$$

which reproduces the qualitative features of (9b).

3. Detection of Signal in the Presence of Noise

The primary source of noise in the interferometer arises from vibrations of the mirrors. As a result of these vibrations, the phase $\phi_{23}$ depends on the time through a fluctuating part, as well as through the signal. Write

$$\phi_{23}^o = \theta_o(t) + n(t), \tag{10}$$

where $\theta_o(t)$ is a slowly varying function of time corresponding to a steady drift of the system, and n(t) is a rapidly fluctuating function of time. Then, making an approximation similar to 9c, one approximates the time-dependent laser intensity by

$$\Delta|u|^2 = I_o\{\cos[\theta_o(t)+n(t)] + \sin[\theta_o(t)+n(t)]\phi'_{23}s(t)\}. \tag{11a}$$

Thus, the signal to be detected has a noisy amplitude, as well as a background of noise. Experimentally, it is possible to make $n(t) \ll 2\pi$, so that the signal may be approximated by

$$\Delta|u|^2 = I_o\{\cos\theta_o(t) - n(t)\sin\theta_o(t) + [\sin\theta_o(t) + n(t)\cos\theta_o(t)]\phi'_{23}s(t)\}. \tag{11b}$$

The first term has no Fourier component at the frequency of s(t), and can be neglected. The intensity of the signal induced by the unknown phase shift is now

$$I_s = I_o[\sin\theta_o(t) + n(t)\cos\theta_o(t)]\,\phi'_{23} \tag{12}$$

which has an average, $I_o \sin\theta_o(t)\,\phi'_{23}$. It is important to note that the noise part of the amplitude goes to zero as $\phi'_{23}$ goes to zero; thus, as measurements are made by setting $\phi_{23}$ zero, the noise affects the sensitivity but not the accuracy of the instrument. If $\theta_o$ is assumed constant, it can be shown[5] that the best measure of the average intensity is

$$\langle I_s \rangle = \frac{\int_0^T \Delta|u|^2\, s(t)\, dt}{\int_0^T s^2(t)\, dt}. \tag{13}$$

This is the detection process used in synchronous detection with, however, one difference.

Because of the time dependence of $\theta_o$, T cannot be longer than that required for $\theta_o$ to change by $\pi$. Thus, the detection technique should be synchronous detection with the integration time limited by the drift time of the apparatus.

4. Phase Compensator

The linear electro-optic effect[6] in crystalline $\alpha$-quartz is used to compensate the unknown dielectric constant. If an electric field is applied along the x axis of the crystal, the dielectric constant for a light wave polarized in the x axis and propagating in the y-direction changes by an amount

$$\Delta n = 1.1 \times 10^{-10} E \tag{14}$$

with E in volts/cm. For these orientations, there is no rotation of the polarization of the light. Experimental evidence[7] shows that the change of the dielectric constant is almost independent of wavelength in the visible region, and it seems likely that this independence continues into the near infrared. The quartz will be calibrated for all wavelengths used in the interferometer.

The crystal used is 10 cm long and 0.5 cm thick, so that if a voltage is applied across the crystal, the phase change is

$$\Delta = \frac{2\pi}{\lambda}(2.2 \times 10^{-9})\ \text{V}. \tag{15a}$$

For operation at the red line of the helium-neon laser, this is

$$\Delta = 2\pi(3.16 \times 10^{-5})\ \text{V}. \tag{15b}$$

A pressure box activated by a loud speaker and the Kerr effect in nitrobenzene were also considered as possible compensators. The Kerr effect was rejected because of the experimental difficulties associated with nitrobenzene, and because higher voltages are required for small phase shifts. The pressure box was rejected because it is undesirable to generate sound waves at the measuring frequency in the vicinity of the interferometer.

5. Experimental Apparatus

The interferometer has been operated at the 0.633 $\mu$ line, the 1.15 $\mu$ line, and the 3.39 $\mu$ line of the helium-neon laser. By operating with the red line, it has been possible to detect phase shifts of approximately $2\pi \times 10^{-3}$ radians, which would correspond to an electron density of $\sim 5 \times 10^{13}$ cm$^{-3}$ along a path length of 10 cm. Thus far, however, the drift of the laser mirrors has made it difficult to obtain a precise null of the unknown signal. As this drift is due to thermal effects, the interferometer is being mounted on invar rather than the present aluminum.

One more modification is intended for the interferometer. To permit studies of time-dependent effects (e.g., afterglows) a gating circuit will be placed between the photodetector and the synchronous amplifier.

E. B. Hooper, Jr.

## References

1. D. E. T. F. Ashby and D. F. Jephcott, Appl. Phys. Letters 3, 13 (1963).

2. J. B. Gerardo and J. T. Verdeyen, Appl. Phys. Letters 3, 121 (1963); Proc. IEEE 52, 690 (1964).

3. G. D. Boyd and J. P. Gordon, Bell Sys. Tech. J. 40, 489 (1961).

4. G. D. Boyd and H. Kogelnik, Bell Sys. Tech. J. 41, 1347 (1962).

5. T. A. Wainstein and V. D. Zubakov, Extraction of Signals from Noise (Prentice-Hall, Inc., Englewood Cliffs, N.J., 1962), Sec. 50.

6. W. G. Cady, Piezoelectricity (McGraw-Hill Publishing Company, Inc., N.Y., 1946).

7. N. Günther, Ann. Physik 13, 783 (1932).